# Display Augmentation in Manual Control of Remotely Piloted Vehicles

S. J. Merhav* and A. J. Grunwald†
*Technion – Israel Institute of Technology, Haifa, Israel*

**The effectiveness of display aids for the manual control of remotely piloted vehicles by television during landing approach is investigated. The task is lateral and vertical control along a required glide-slope trajectory in the presence of lateral and vertical random disturbances. By superimposing suitable glide-slope reference lines on the TV monitor, the glide-slope error can be derived directly from the visual field. It is theoretically investigated whether and under what conditions the display of higher-order state components, such as the vertical velocity and/or acceleration, is required. It is shown that, for a body-mounted camera, essential angular rate information can be detected from the vertical relative motion of the visual field due to vehicle pitching. This information is required, in particular, for relatively slow vehicle dynamics. On the other hand, rapid pitching, which occurs with fast vehicle dynamics, may be detrimental to its effective control. These disturbing motions can be easily eliminated by a gyro-stabilized camera, but then the essential angular and pitch information is also eliminated and control becomes difficult. A display configuration is, therefore, proposed in which position, rate, and acceleration cues are derived from a single error displayed by special reference bars. It is theoretically and experimentally shown that the effectiveness of the display configuration and the type of camera mounting (body-mounted or inertially stabilized) is highly dependent on vehicle dynamics and disturbance bandwidth.**

## Nomenclature

$\Gamma_0$ = required glide-slope angle
$\Gamma$ = glide-slope error
$h_0$ = height of the aircraft above the ground
$h$ = vertical deviation from the required glide-slope
$V$ = velocity vector
$\gamma$ = vertical path angle
$\theta$ = pitch angle
$\alpha$ = angle of attack
$R$ = distance of the aircraft from the glide-slope/runway intersection point

## I. Introduction

THE manual landing approach of remotely piloted vehicles RPV's by means of an airborne TV camera encounters similar difficulties as the lateral control task discussed in Refs. 1 and 2. These difficulties can be attributed to the narrow visual field (VF) and the lack of motion cues. In Ref. 2, some basic ground rules are proposed for the design of simple display aids for lateral RPV control, which should be superimposed on the TV monitor image. In this paper, these ground rules are implemented to the landing approach of RPV's. The control task involves keeping the vehicle on a required glide slope. A side view of the location of the vehicle in a vertical plane is shown in Fig. 1a.

The glide-slope error is defined as

$$\Gamma = h/R \tag{1}$$

With sophisticated and expensive landing systems, the glide-slope error $\Gamma$ is usually detected with the aid of a ground station and localizer beam. $\Gamma$ is explicitly shown on a display, and the display gain can be chosen in accordance with the accuracy at which the glide slope must be followed. Glide-slope control with visual field cues only, and without vehicle-based reference lines, is based on the estimation of the height $h_0$ and the range $R$ from the apparent size and geometrical form of the runway.

Naish,[3] considering human threshold effects, found these visual field cues highly inaccurate and attempted to provide additional positional and flight-path information by superposition of conformal guidance symbology on the visual field by means of head-up display techniques.[4,5] Van Houtte[6] and Palmer and Wempe[7,8] proposed computer-generated pictorial landing display systems. Palmer and Wempe investigated guidance symbology, such as flight directors, flight-path information, etc., to be added to the basic perspective runway image in the different stages of the approach. Howard[9,10] investigated superimposed display aids in the visual RPV approach to landing.

RPV technology, however, facilitates augmentation of the TV monitor image by glide-slope reference lines, enabling

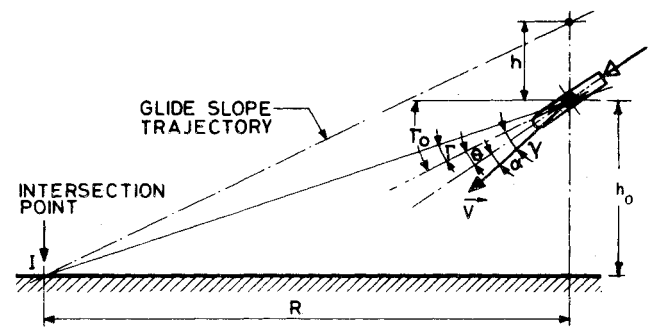


Fig. 1a) Side view of the landing approach.

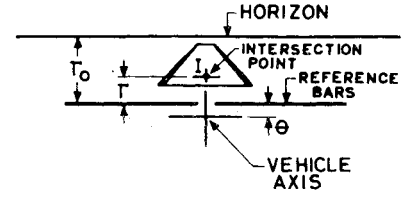


Fig. 1b) TV monitor image of the landing approach.

Received Sept. 16, 1977; revision received Nov. 28, 1977. 

Index categories: Guidance and Control; Handling Qualities, Stability and Control; Human Factors.

*Professor, Control Systems Engineering, Dept. of Aeronautical Engineering.

†Presently, Postdoctoral Fellow, NASA Langley.

detection of $\Gamma$ directly from the VF. These reference lines are depressed $\Gamma_0$ deg below the true horizon, as shown in Fig. 1b. The necessary signals for positioning these lines can readily be obtained from a vehicle-mounted pitch gyro. $\Gamma$ is thus detected as the visual angle, subtended between these reference lines and the glide-slope intersection point. In contrast with instrument displays, $\Gamma$ is obtained here without the need for measuring $R$ and $h_0$ or a localizer beam. However, the glide-slope error gain is determined by the VF geometry and, thus, cannot be chosen freely. In this paper, the usefulness of these superimposed reference lines is theoretically and experimentally investigated for two basic camera mountings – a body-mounted camera and an inertially-stabilized camera.

Similar to lateral RPV control of Ref. 2, the TV monitor image can be augmented easily by the display of higher-order state components, such as the vertical velocity and/or acceleration of the vehicle. It is experimentally investigated whether and under what conditions the human operator actually utilizes this information of higher-order state components, and to what extent the augmented display improves control performance.

## II. Theoretical Analysis

### A. The Vehicle Model

A roll-stabilized vehicle is considered. The forward velocity $V$ is assumed to be constant and thus only the short-period vehicle dynamics are represented. The longitudinal and lateral vehicle dynamics are then identical. Figure 2 represents a side view of the vehicle with the associated forces and moments to which it is subjected. Since small perturbations about the reference trajectory are considered, the lift force $F_w$ is assumed to be proportional to $w$, in accordance with $F_w/m = Z_w w$, where $m$ is the vehicle mass and $Z_w$ is defined as the vertical gain. Similar proportional relationships are defined for the angle-of-attack stability moment and the pitch damping moment according to $T_w/I_y = M_w w$ and $T_q/I_y = M_q q$, where $q$ is the pitch rate, $I_y$ is the moment of inertia of the vehicle about the $y$ axis, and $M_w$ and $M_q$ are defined as the angle-of-attack stability gain and pitch damping gain, respectively. The equations of motion and transfer functions are derived in the Appendix.

### B. Vertical Glide-Slope Control with a Body-Mounted Camera

*1. Fixed Reticle*

It is assumed that control about the glide slope is accomplished by keeping the vehicle axis in the direction of the intersection point. This involves keeping the intersection point $I$ on a fixed reticle indicated on the monitor image. The control error for relatively small values of $h$ and $\Gamma_0$ is then given by

$$\epsilon = \theta + \Gamma = \theta + h/R \tag{2}$$

(see Fig. 1a), and with Eqs. (A7, A9, and A10) in the Appendix, the transfer function of the controlled element (vehicle + VF) can be written as

$$H^{\epsilon}_{\delta}(s) = \frac{M_\delta [s^2 + Z'_w s + Z'_w V/R]}{s^2 [s^2 + (Z_w + M_q)s + Z_w M_q + M_w V]} \tag{3}$$

where

$$Z'_w = Z_w - M_w (Z_\delta / M_\delta) \tag{4}$$

Equation (3) shows that $H^{\epsilon}_{\delta}(s)$ has two poles at the origin, two poles determined by the vehicle parameters, and two zeros determined by $Z'_w$ and $V/R$. Since $R$ is a function of time, the location of these zeros changes during the approach. At the beginning of the glide slope $V/R$ is small, so that one zero is close to the origin and one is at $s = -Z'_w$, yielding a closed-loop system with one pole close to the origin. This results in a large error in $h$, if the vehicle is subjected to strong, low-frequency disturbances, e.g., a constant updraft. Only at the end of the glide slope will the zero be sufficiently removed from the origin to enable the error in $h$ to be corrected. Therefore, a fixed reticle is an inadequate display aid for keeping the vehicle on the glide slope.

*2. Glide-Slope Reference Lines*

For glide-slope control with reference lines, the control error $\epsilon$ is equal to $\Gamma$. $H^{\epsilon}_{\delta}(s)$ follows from Eqs. (1) and (A9), and is given by

$$H^{\epsilon}_{\delta}(s) = \frac{(1/R) M_\delta Z'_w V - (1/R) Z_\delta s (s + M_q)}{s^2 \Delta(s)} \tag{5}$$

with $\Delta(s)$ given by Eq. (A10). Generally, since $z_\delta \ll M_\delta$, the zeros in Eq. (5) are far away from the origin, so that the control of this fourth-order system is nearly impossible without rate information, particularly, if the two poles of the vehicle dynamics are close to the origin. A block diagram of the control system is shown in Fig. 3.

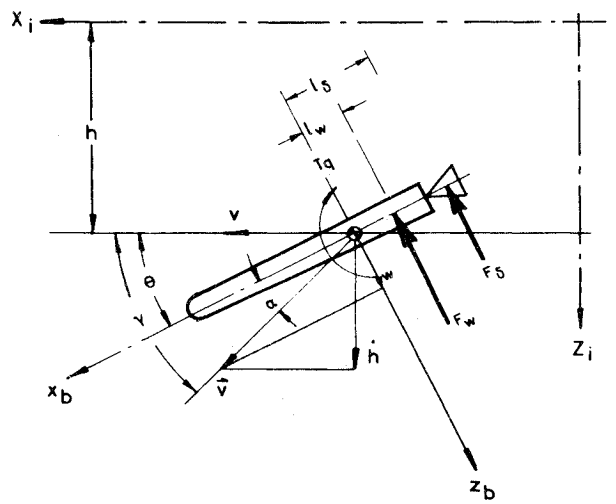


Fig. 2 Side view of vehicle with forces and moments. For small $\theta$ and $\alpha$, $\dot{h}/V \approx \theta + \alpha$, $w/V \approx \alpha$.

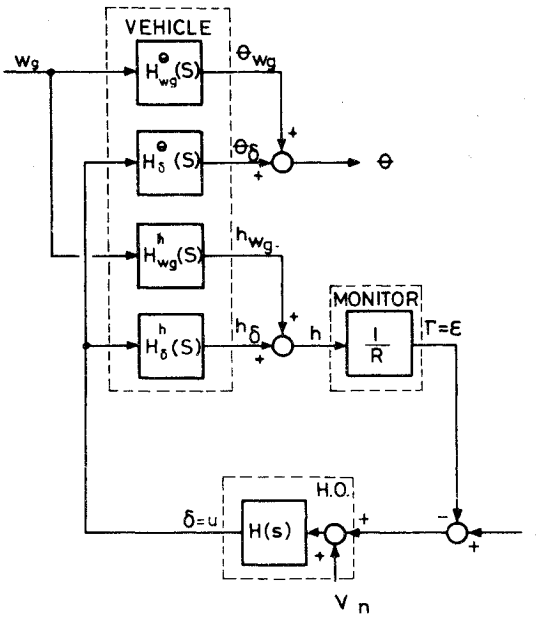


Fig. 3 Block diagram of the control system for glide-slope control with reference bars.

The human operator (HO) transfer function is represented by $H(s)=N(s)/D(s)$ and the HO remnant source, combining observation and motor noise, by $v_n(s)$. According to Weir and McRuer,[11] the basic structure of $H(s)$ consists of a gain, a lead-lag adaptive term, a neuromuscular lag, and a time delay. From Fig. 3 and with Eqs. (A9) and (A13), an expression for the closed-loop power spectrum of $\Gamma$ can be derived from

$$\Gamma(s)=\frac{-(1/R)Z_w s(s+M_q)D(s)}{D_{cl}(s)}w_g(s)$$

$$+\frac{(1/R)\,[M_\delta Z'_w V-Z_\delta s(s+M_q)\,]N(s)}{D_{cl}(s)}v_n(s) \qquad (6)$$

where $D_{cl}$ is the denominator of the closed-loop system. Equation (6) shows that $v_n(s)$ is strongly filtered since $Z_\delta \ll M_\delta$, and that the filtering of $w_g(s)$ depends on $M_q$. Therefore, the $\Gamma$ spectrum will have little high-frequency power. Apart from this, the static gain of $\Gamma$ is small due to the relatively large value of $R$. Therefore, rate estimation from $\Gamma$ will be quite difficult.

With a body-fixed camera, rate cues are, to some extent, derived from the pitch motion of the vehicle. It follows from Eqs. (A7) and (A9) that with zero disturbances and $Z_\delta \ll M_\delta$, $\Gamma$ and $\theta$ are related by a first-order lag in accordance with

$$\frac{s\Gamma(s)}{\theta(s)}=\frac{(V/R)Z'_w}{(s+Z'_w)} \qquad (7)$$

It will be shown experimentally in Sec. III.B that control of the fourth-order system of Eq. (5) is still possible by virtue of the rate information $\dot{\Gamma}=\dot{h}/R$ provided by $\theta$. However, the pitch cues have the following shortcomings

a. Limited Control Gain: Equation (7) shows that for small $Z_w$ and large $R$, a large pitch angle is needed to obtain the required response of $\dot{\Gamma}$. However, $\theta$ is limited by the field-of-view of the camera, thus limiting the control gain. If a larger pitch angle is required, for instance, in the presence of powerful disturbances, loss of control will occur.

b. Increased Observation Noise: Rapid $\theta$ motions will result in increased observation noise in the perception of $\Gamma$. With the block diagram of Fig. 3 and Eqs. (A7, A9, A11, and A13), the following expression for the closed-loop power spectrum of $\theta$ can be found:

$$\theta(s)=\frac{M_w s^2 D(s)+(1/R)M_\delta Z'_w N(s)}{D_{cl}(s)}w_g(s)$$

$$+\frac{M_\delta(s+Z'_w)sN(s)}{D_{cl}(s)}v_n(s) \qquad (8)$$

As expected, Eq. (8) shows that the $\theta$ spectrum has more high-frequency power than the $\Gamma$ spectrum. The high-frequency power, yielding rapid pitch motions, depends mainly on $M_w$.

### C. Vertical Glide-Slope Control with an Inertially Stabilized Camera

*1. Independently Steerable Camera*

The pitch, yaw, and roll motion of an inertially stabilized camera can be controlled independently and completely decoupled from vehicle motions. Thus, the pitch angle of the camera can be preset $\Gamma_0$ deg below the true horizon. The glide-slope reference lines are indicated by fixed reference lines on the monitor image. Glide-slope control now involves keeping the intersection point on these reference lines. Apart from the missing pitch motion, the control task is identical to the task with a body-mounted camera. In Sec. III.B, it is experimentally confirmed that elimination of the pitch motion is advantageous for fast vehicle dynamics. However, if the short-period pole pair is close to the origin, the rate information provided by the $\theta$ motion is essential, so that the isolation of the pitch motion from the display may be detrimental.

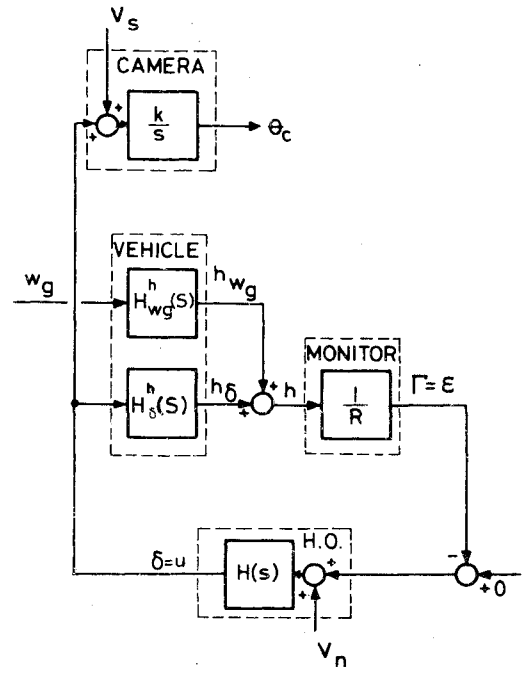


**Fig. 4 Block diagram of the control system for glide-slope control with a rate-controlled inertially stabilized camera.**

*2. Rate-Controlled Inertially Stabilized Camera*

With an inertially stabilized rate-controlled camera, the camera pitch rate $\dot{\theta}_c$ is made proportional to the control command according to $\dot{\theta}_c=K\delta$. This mode of control is commonly used for terminal guidance tasks. For glide-slope control, the structure of the control system is shown in Fig. 4. The addition of noise, indicated in Fig. 4 by $v_s$, accounts for the offset and inaccuracy in the positioning of the camera. The relationship $\dot{\Gamma}/\theta_c$ assuming $Z_\delta \ll M_\delta$, is given by

$$\frac{s\Gamma(s)}{\theta_c(s)}=\frac{(1/KR)M_\delta Z'_w V}{\Delta(s)} \qquad (9)$$

Equation (9) shows that $\theta_c$ also provides some rate information $\dot{\Gamma}=\dot{h}/R$, having a large phase lag for slow vehicle dynamics. The usefulness of the camera motion $\theta_c$ is, therefore, questionable, since rate information is the most needed for slow vehicle dynamics. From Fig. 4 and with Eqs. (A9) and (A13), an expression for the closed-loop power spectrum of $\theta_c$ can be derived:

$$\theta_c(s)=\frac{Ks\Delta(s)N(s)}{D_{cl}(s)}v_n(s)$$

$$+\frac{(K/R)Z_w(s+M_q)N(s)}{D_{cl}(s)}w_g(s)+\frac{K}{s}v_s(s) \qquad (10)$$

Equation (10) shows that the $\theta_c$ spectrum has little high-frequency power, since $w_g$ is strongly filtered. However, since $v_s$ is integrated, a slow drift of $\theta_c$ will result. Loss of control occurs if $\theta_c$ exceeds the field-of-view of the camera. Therefore a rate-controlled camera is not suitable for glide-slope control.

### D. Display Augmentation by Rate and Acceleration Cues

*1. Velocity-Vector Symbol*

In Secs. II.B.2 and II.C, it is shown that not in all cases can rate information be obtained from the pitch motion of the camera. However, the monitor display can be easily

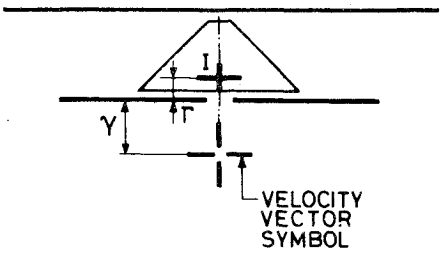


Fig. 5 Monitor image with glide-slope reference bars and velocity-vector symbol.

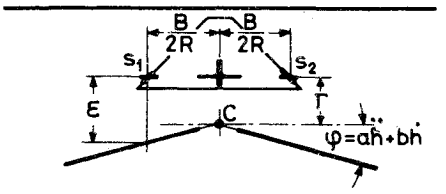


Fig. 6 Monitor image with augmented glide-slope reference bars.

augmented by rate and/or acceleration cues. Kleinman[12] found that augmentation of a glide-slope display by a velocity-vector symbol is useful for a relatively heavy aircraft, such as the DC-8.

Figure 5 shows the display with glide-slope reference lines and a velocity-vector symbol. The control task involves keeping the velocity-vector symbol on the intersection point $I$. The control error is then defined as

$$\epsilon = \gamma + \dot{h}/R \tag{11}$$

or

$$\epsilon(s) = (1/V)(s + V/R)h(s) \tag{12}$$

Due to the relatively small $V/R$ ratio, the zero in Eq. (12) is close to the origin, thus giving rise to a large glide-slope error. Therefore, keeping the velocity-vector symbol on the intersection point is not necessarily a sufficient control strategy. The vertical path angle $\gamma = \dot{h}/R$ is indicated on the monitor in Fig. 5 as the deviation of the velocity-vector symbol from the glide-slope reference lines. This rate information may well serve as an inner rate loop closure, but an outer positional loop closure is still required to implement glide-slope control. A disadvantage of this display configuration is that both rate and positional cues $\gamma$ and $\Gamma$ have to be perceived and processed independently.

*2. Glide-Slope Reference Lines Augmented by Rate and Acceleration Information*

A display configuration was sought in which positional, rate, and acceleration cues are included in a single control error. Such a configuration is shown in Fig. 6. Rate and acceleration cues originate here from the rotation of the glide-slope reference lines about the point $C$. The angle of rotation $\varphi$ is determined by $\varphi = a\ddot{h} + b\dot{h}$ where $a$ and $b$ are proportionality constants. $\ddot{h}$ can be measured on board by an accelerometer and $\dot{h}$ by measuring $\alpha$ and $\theta$, since $\ddot{h} = (\alpha + \theta)V$, or by direct measurements. It follows from Fig. 6 that the control error for a point $s_1$ on the runway guideline, a distance $\frac{1}{2}B$ off the intersection point, is given by

$$\epsilon = a(B/2R)\ddot{h} + b(B/2R)\dot{h} + h/R \tag{13}$$

or

$$\epsilon(s) = (1/R)[(aBs^2/2) + (bB/2)s + 1]h(s) \tag{14}$$

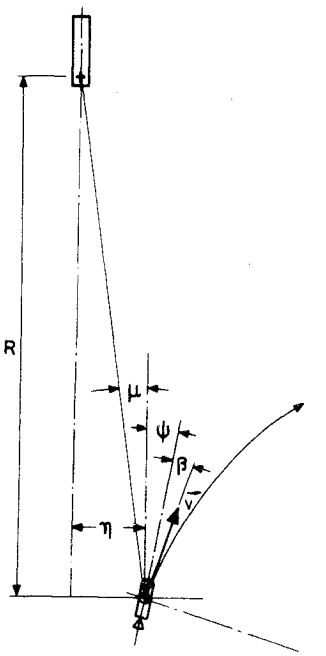


Fig. 7a Plan view of the landing approach.

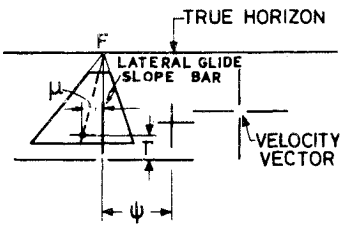


Fig. 7b Monitor image.

where $B$ is the runway width. Equation (14) shows the presence of a second-order lead term, independent of vehicle or VF parameters. The location of the zeros is independent of $R$ and, thus, does not change during the approach. The proportionality constants $a$ and $b$ can be calibrated for a given $B$ and $V$ so that the two zeros yield a stable and well-damped system. The control task then simply involves the alignment of the augmented glide-slope reference lines with the points $s_1$ and $s_2$.

It should be noted that with this display configuration, glide-slope control, as well as the creation of zeros independent of $R$, is achieved by proper use of the VF cues, without the need for measuring $R$ or $h$.

**E. Lateral and Combined Lateral-Vertical Glide-Slope Control**

Figure 7 shows a plan view of the landing approach. The control task involves keeping the vehicle laterally on the glide slope. The necessary VF information is mainly derived from the runway centerline which, however, is only indicated for a looking distance $D > R$. Since, numerically, $V \ll R$, the $V/D$ ratio is limited to a relatively small value. In Refs. 1 and 2, it is shown that lateral control display aids, such as a fixed reticle, velocity-vector reticle, or vehicle-path reticle will not be useful for small values of $V/D$, since the controlled element will have a zero close to the origin.

A display aid more suitable for lateral glide-slope control is a lateral glide-slope bar, as shown in Fig. 7b, indicating the direction of the glide-slope reference trajectory. This information may be obtained from an onboard directional gyro or compass. The lateral glide-slope error $\mu = \eta/D$ is then defined as the visual angle, subtended between the intersection point and the lateral glide-slope bar. Lateral slope control is then identical to longitudinal glide-slope control, so that the analysis in Secs. II.A-II.D is valid for lateral glide-slope control as well.

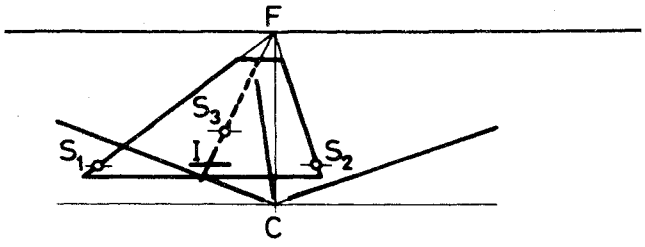


**Fig. 8 Combined display configuration with augmented lateral and vertical.**

As in the vertical case, the lateral glide-slope line for an inertially stabilized camera is also indicated by a fixed reticle. Prior to entering the glide slope, the camera axis is directed parallel to the direction of the glide slope, and control is accomplished by alignment of intersection point and fixed reticle, indicating the camera axis.

By rotation of the lateral glide-slope bar about the same center $C$ as the two longitudinal glide-slope bars, lateral rate and acceleration cues can be displayed. The combined display configuration is shown in Fig. 8. In order to accomplish lateral control, a third reference point $s_3$ must be indicated on the runway centerline. Similar to the vertical case, two zeros, independent of $R$, are thus obtained.

It is of particular interest whether the HO is able to use these displayed higher-order cues in the combined lateral-vertical glide-slope control task. Due to the increased task complexity, improperly processed higher-order information might result in a deterioration of performance. The experimental results of the combined task are discussed in Sec. III.B.2.

## III. Experimental Program

### A. Description of the Experiments

The experiments involve the following data:

| | |
|---|---|
| forward velocity (constant during the approach) | $V = 42.5$ m/s |
| required glide-slope angle | $\Gamma_0 = 13.2$ deg |
| initial height | $h_{0_i} = 720$ m |
| initial range | $R_i = 3000$ m |
| average rate of descent | $= 10.2$ m/s |
| final height | $= 108$ m |
| final range | $= 450$ m |

The purpose of the program was to investigate the effectiveness of the display configuration proposed in Sec. II.E for body-mounted and inertially stabilized cameras, for various vehicle dynamics and disturbance spectra, and to validate the theoretical considerations given in Sec. II. In this program the same RPV simulator as in Refs. 1 and 2 has been used.

The field-of-view of the camera is $\pm 10$ deg horizontally and $\pm 7.5$ deg vertically. The reference bars are straight bright lines superimposed on the TV monitor image. The control task is to minimize the vertical or vertical-plus-lateral glide-slope error. The monitor is positioned 2.50 m from the operator. Each approach started with an initial glide-slope error of 0.55 deg and lasted 1 min.

Two subjects participated in the experimental program. Subject 1 had previous extensive simulator training with compensatory tracking tasks and lateral vehicular RPV control, and performed ~20 training runs of 1 min each. Subject 2 had no previous simulator training and underwent ~120 training runs of 1 min each. Both subjects yield basically the same results. Only the results for the first subject are presented in this paper.

The variances of $\theta$, $h$, and the control force $u$ were measured and normalized with respect to the variance of $w_g$. The rms value of $w_g$ was about 3 m/s. In all experiments, $w_g$ was first-order bandlimited white noise with the bandlimit at 1.5 Hz. Three break frequencies were considered: 0.1, 0.4, and 1.6 rad/s. The constants $a$ and $b$ of the augmented glide-slope bars were calibrated so that the two zeros were located at $S_{1,2} = 0.5 \pm 0.5j$.

### B. Results

*1. Vertical Glide-Slope Control*

The experimental results for three pole-zero configurations are shown in Figs. 9-11. The vehicle parameters determining the three configurations are summarized in Table 1. The normalized pitch, height, and control variances $V_\theta$ (deg/m-s$^{-1}$)$^2$, $v_h$ (m/m-s$^{-1}$)$^2$, and $v_u$ (deg/m-s$^{-1}$)$^2$ were determined as a function of the disturbance break frequency $a_f$, for $a_f = 0.1$, 0.4, and 1.6 rad/s. Results for four camera display situations at $a_f = 0.4$ rad/s are shown. The results for the other values of $a_f$ do not differ significantly. Each point represents the average of a set of six to twelve 1-min runs. The vertical lines indicate the standard deviation of the set. The experimental results are summarized below.

a. Results for Configuration 1: Configuration 1 represents the dynamics of a Navion low-wing light aircraft, with $Z_w = -2.024$ (rad-s)$^{-1}$ and two vehicle poles at $s_{1,2} = -2.05 \pm 2.96j$. Figure 9 shows that:

1) Both the pitch and control variances $V_\theta$ and $V_u$ for the inertially stabilized camera are considerably higher than for the body-mounted camera, indicating poor damping and large overshoots. This indeed confirms the assumption of Sec. II.B.2 that essential rate information is derived from the pitch motion, and thus contributes to the stability of the system, in particular, for the relatively slower RPV vehicle dynamics.

2) For the body-mounted camera, augmentation of the glide-slope reference bars by the higher state components yields lower values of $V_\theta$, $V_h$, and $V_u$. This confirms that, in addition to the rate information provided by the pitch motion, the higher-order information imparted to the glide-slope bars is also used.

3) A stabilized camera with augmented glide-slope reference bars yields a performance very similar to the body-mounted camera. This demonstrates that the rate information, lost as a result of the elimination of the pitch motion, can be effectively reestablished by the augmented glide-slope lines. For the stabilized camera with augmented lines, the variances are even slightly lower, probably because the higher-order information is perceived directly, whereas

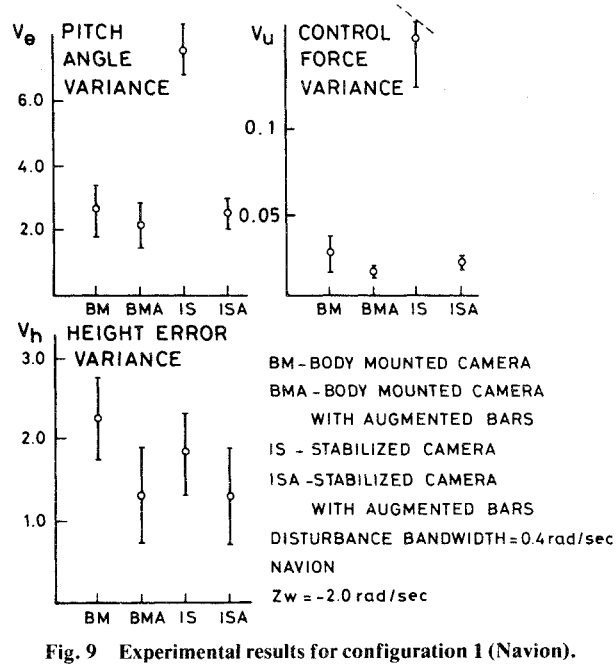


**Fig. 9 Experimental results for configuration 1 (Navion).**

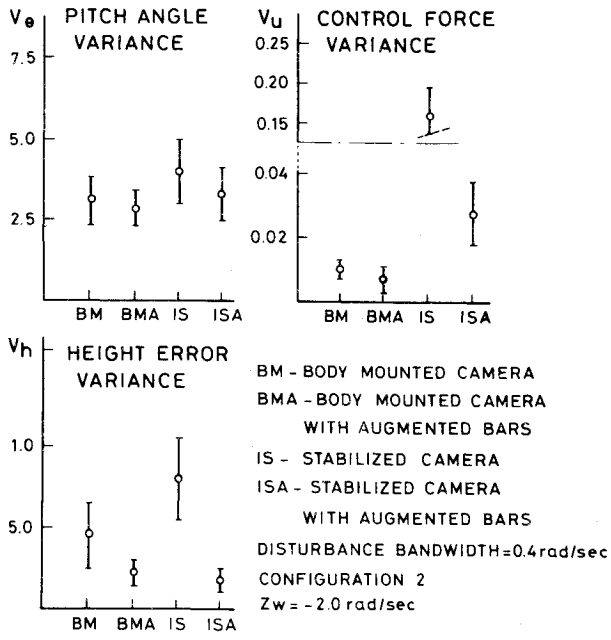


Fig. 10 Experimental results for configuration 2.

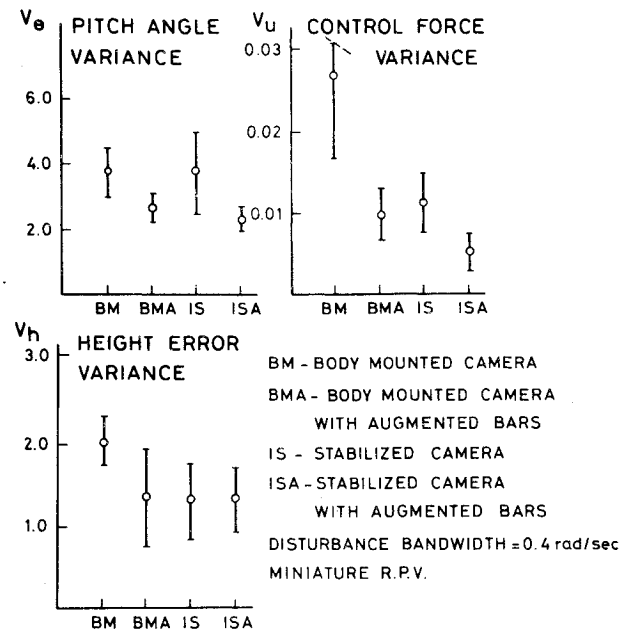


Fig. 11 Experimental results for configuration 3.

**Table 1 Parameter values of longitudinal vehicle dynamics and display constants**

| | $V$, m/s | $Z_\delta$,[a] m-s$^{-2}$/deg | $Z_w$, 1/rad-s | $M_\delta$, rad-s$^{-2}$/deg | $M_w$, 1/m-s | $M_q$, 1/s | Vehicle dynamics poles, $s_{1,2}$ | Display constants $a$, s$^2$/m | $b$, s/m | Runway width $B$, m |
|---|---|---|---|---|---|---|---|---|---|---|
| I (Navion) | 42.5 | 0.358 | 2.024 | 0.575 | 0.206 | 2.077 | $-2.05 \pm 2.96j$ | | | |
| II | 42.5 | 0. | 2.0 | 0.26 | 0.047 | 0. | $-1 \pm j$ | 0.08 | 0.08 | 50 |
| III (Mini RPV) | 42.5 | 0.406 | 7.14 | 2.43 | 1.575 | 2.1 | $-4.6 \pm 7.8j$ | | | |

[a] deg = degree control stick deflection

**Table 2 Experimental results for vertical and combined glide-slope control**

| | | Configuration 1 (Navion) | | | Configuration 2 | | | Configuration 3 (miniature RPV) | | |
|---|---|---|---|---|---|---|---|---|---|---|
| | | $V_\theta$[a] | $V_h$ | $V_u$ | $V_\theta$ | $V_h$ | $V_u$ | $V_\theta$ | $V_h$ | $V_u$ |
| BM[b] | $V$[c] | 2.60[d] | 2.25 | 0.034 | 3.10 | 4.56 | 0.010 | 3.78 | 2.07 | 0.027 |
| | | ±0.80 | ±0.052 | ±0.011 | ±0.83 | ±2.59 | ±0.003 | ±0.78 | ±0.32 | ±0.012 |
| | $C$ | 2.76 | 2.07 | 0.049 | 4.79 | 2.97 | 0.027 | 3.94 | 2.60 | 0.028 |
| | | ±0.78 | ±0.59 | ±0.001 | ±1.98 | ±1.13 | ±0.009 | ±0.78 | ±1.39 | ±0.006 |
| BMA | $V$ | 2.14 | 1.30 | 0.013 | 2.89 | 2.43 | 0.0074 | 2.71 | 1.36 | 0.010 |
| | | ±0.07 | ±0.78 | ±0.001 | ±0.54 | ±0.84 | ±0.0046 | ±0.56 | ±0.69 | ±0.003 |
| | $C$ | 1.87 | 1.60 | 0.020 | 2.70 | 1.71 | 0.010 | 2.89 | 1.67 | 0.0089 |
| | | ±0.39 | ±0.64 | ±0.005 | ±0.43 | ±0.59 | ±0.002 | ±1.07 | ±1.11 | ±0.0041 |
| IS | $V$ | 7.64 | 1.82 | 0.158 | 3.98 | 8.60 | 0.173 | 3.81 | 1.31 | 0.011 |
| | | ±0.82 | ±0.51 | ±0.037 | ±1.20 | ±3.20 | ±0.066 | ±1.25 | ±0.46 | ±0.003 |
| | $C$ | 8.63 | 3.86 | 0.170 | Impossible to control | | | 6.54 | 1.85 | 0.045 |
| | | ±2.92 | ±0.14 | ±0.007 | | | | ±2.25 | ±0.76 | ±0.011 |
| ISA | $V$ | 2.55 | 1.39 | 0.019 | 3.33 | 1.90 | 0.028 | 2.40 | 1.34 | 0.0054 |
| | | ±0.55 | ±0.49 | ±0.003 | ±0.81 | ±0.67 | ±0.013 | ±0.39 | ±0.39 | ±0.002 |
| | $C$ | 3.05 | 2.47 | 0.028 | 11.20 | 5.36 | 0.113 | 2.74 | 1.36 | 0.0086 |
| | | ±1.10 | ±0.74 | ±0.011 | ±5.55 | ±3.33 | ±0.069 | ±1.02 | ±0.32 | ±0.0029 |

[a] $V_\theta$ (deg/m-s$^{-1}$)$^2$, $V_h$ (m/m-s$^{-1}$)$^2$, $V_u$ (deg/m-s$^{-1}$)$^2$ – pitch, altitude, and control variances, respectively.
[b] BM, body-mounted camera; BMA, body-mounted camera with augmented bars; IS, inertially stabilized camera; ISA, inertially stabilized camera with augmented bars.
[c] $V$, vertical control task; $C$, combined lateral-vertical task.
[d] Each result is the average of twelve 1-min runs.

with the body-mounted camera, the rate information is perceived with a first-order lag.

b. Results for Configuration 2: Configuration 2 represents an aircraft heavier than the Navion with $Z_w = -2$ (rad-s)$^{-1}$ and two vehicle poles at $s_{1,2} = -1 \pm j$.

The results in Fig. 10 show that for the stabilized camera, $V_\theta$, $V_h$, and $V_u$ are very large, indicating a poorly damped system resulting in low system performance. Augmented glide-slope lines are able to reestablish part of the necessary higher-order information, but for a body-mounted camera $V_\theta$ and $V_u$ are still lower. Also, for this configuration a body-mounted camera with augmented lines yields the best performance.

c. Results for Configuration 3: Configuration 3 represents

a miniature RPV with $Z_w = -7.14$ (rad-s)$^{-1}$ and two vehicle poles at $s_{1,2} = -4.6 \pm 7.8\,j$. With $M_w = -1.58$ (m-s)$^{-1}$, the $\theta$ spectrum has a high bandwidth, as can be shown by Eq. (8). The results in Fig. 11 show:

1) The body-mounted camera yields the largest values of $V_u$ and $V_h$. Most likely this is caused by the rapid pitch motions which result in increased observation noise.

2) For the body-mounted camera, augmented glide-slope lines yield considerably lower values of $V_\theta$ and $V_u$ than regular lines. This demonstrates that, in spite of the rapid pitch motions, the higher-order information provided by the augmented lines is successfully used.

3) A stabilized camera with augmented lines yields the best performance. The fast pitch motions are eliminated and the higher-order information is successfully provided by the augmented lines. Even for this rapidly responding vehicle, higher-order information is shown to be useful, since it includes information about the disturbance, enabling the execution of a counteracting control action before a sizable glide-slope error develops.

*2. Combined Lateral-Vertical Glide-Slope Control Task*

In the combined glide-slope control task, the lateral and vertical vehicle dynamics are assumed to be identical and completely decoupled. The rms value of the lateral disturbance $v_g$ was about 2.25 m/s and the vertical disturbance 3 m/s. The filter break frequency in all cases was 0.4 rad/s. The constants $a$ and $b$ related to the lateral augmented glide-slope line were calibrated so that two zeros at $s_{1,2} = -0.5 \pm 0.5j$ were obtained. The results for the three vehicle configurations for combined control and vertical control only are presented in Table 2. Each result represents the average of a set of 12 approaches of 1-min duration and are summarized as follows:

1) The results of the combined task show similar characteristics as the vertical task, but are more pronounced. Thus, for all three vehicle configurations, the relative improvement of performance with augmented lines is larger for the combined task than for the vertical task only. This indicates that for the combined task the display of higher-order information is successfully used.

2) The stabilized camera yields a strongly deteriorated performance, in particular, for the combined task. This shows that combined control becomes particularly difficult if rate information is missing. For all three vehicle configurations, augmented glide-slope lines yield a strongly-improved performance.

## IV. Conclusions

1) The experiments confirm the theoretical analysis showing that system performance for a given display configuration and camera system strongly depends on the utilization of higher-order information by the HO.

2) The proposed combined augmented display is feasible for RPV lateral and vertical glide-slope control, and can be realized by utilizing standard onboard instrumentation.

3) An inertially stabilized camera yields inadequate system performance for vehicle dynamics with $\omega_n < \sqrt{2}$ rad/s, since essential rate information is missing. However, this information can be successfully reestablished by augmenting the glide-slope reference lines by higher-order information.

4) For a body-mounted camera, the higher-order information, imparted to the glide-slope reference lines, yields improved system performance for slow as well as fast vehicle dynamics.

5) A body-mounted camera is disadvantageous for vehicle dynamics with $\omega_n > 7$ rad/s because of the rapid pitch motions.

6) The field-of-view for a body-mounted camera should be chosen in accordance with the maximum required pitch angle for a given disturbance spectrum.

7) In the combined lateral-vertical glide-slope control task, the higher-order information imparted to the glide-slope bars is successfully used, and yields a considerably improved system performance.

## Appendix

The vehicle is subjected to the following forces and moments (Fig. 2):

$F_\delta$ = vertical component of the thrust
$F_w$ = lift force
$T_\delta$ = thrust moment about the $y_b$ axis
$T_w$ = angle-of-attack stability moment
$T_q$ = pitch damping moment

The equations of motion are given by

$$I_y \ddot{\theta} = T_\delta + T_w - T_q \tag{A1}$$

$$m\ddot{h} = -F_\delta - F_w \tag{A2}$$

where $\dot{\theta} \triangleq q$, $m$ is the vehicle mass, and $I_y$ the moment of inertia of the vehicle about the $y_b$ axis. For small perturbations about the glide-slope trajectory, the forces and moments are given by

$$F_\delta / m = Z_\delta \delta \tag{A3a}$$

$$F_w / m = Z_w (w - w_g) \tag{A3b}$$

$$T_\delta / I_y = M_\delta \delta \tag{A3c}$$

$$T_w / I_y = M_w (w - w_g) \tag{A3d}$$

$$T_q / I_y = M_q q \tag{A3e}$$

With Eqs. (A3a-A3e), Eqs. (A1) and (A2) can be written as

$$\ddot{\theta} = M_\delta \delta + M_w (w - w_g) - M_q q \tag{A4}$$

$$\ddot{h} = -Z_\delta \delta - Z_w (w - w_g) \tag{A5}$$

where $w = V\alpha$ and $\dot{h} = V(\alpha + \theta)$. The state vector is defined as $x \triangleq \mathrm{col}[q\ \theta\ \alpha\ h]$, and Eqs. (A4) and (A5) can be written as

$$\begin{bmatrix} \dot{q}(t) \\ \dot{\theta}(t) \\ \dot{\alpha}(t) \\ \dot{h}(t) \end{bmatrix} = \begin{bmatrix} -M_q & 0 & M_w V & 0 \\ 1 & 0 & 0 & 0 \\ -1 & 0 & -Z_w & 0 \\ 0 & V & V & 0 \end{bmatrix} \begin{bmatrix} q(t) \\ \theta(t) \\ \alpha(t) \\ h(t) \end{bmatrix} + \begin{bmatrix} M_\delta \\ 0 \\ -Z_\delta / V \\ 0 \end{bmatrix} \delta(t) + \begin{bmatrix} M_w \\ 0 \\ -Z_w / V \\ 0 \end{bmatrix} w_g(t) \tag{A6}$$

From Eq. (A6), the following transfer functions can be derived:

$$H_\delta^q(s) = \frac{q(s)}{\delta(s)} = \frac{M_\delta s + M_\delta Z_w - Z_\delta M_w}{\Delta(s)} \tag{A7}$$

$$H_\delta^\alpha(s) = \frac{\alpha(s)}{\delta(s)} = \frac{-(Z_\delta / V)s - (Z_\delta / V)M_q - M_\delta}{\Delta(s)} \tag{A8}$$

$$H_\delta^h(s) = \frac{h(s)}{\delta(s)} = \frac{-Z_\delta s^2 - Z_\delta M_q s - Z_\delta M_w V + Z_w M_\delta V}{s^2 \Delta(s)} \tag{A9}$$

$$\Delta(s) = [s^2 + (Z_w + M_q)s + Z_w M_q + M_w V] \quad \text{(A10)}$$

$$H^q_{wg}(s) = \frac{q(s)}{w_g(s)} = \frac{M_w s}{\Delta(s)} \quad \text{(A11)}$$

$$H^\alpha_{wg}(s) = \frac{\alpha(s)}{w_g(s)} = \frac{-(Z_w/V)s - (Z_w/V)M_q - M_w}{\Delta(s)} \quad \text{(A12)}$$

$$H^h_{wg}(s) = \frac{h(s)}{w_g(s)} = \frac{-Z_w s^2 - Z_w M_q s}{s^2 \Delta(s)} \quad \text{(A13)}$$

The noise process is modeled by passing zero-mean Gaussian white noise $w$, with covariance $W$, through the first-order filter

$$\dot{w}_g = -a_f w_g + w \quad \text{(A14)}$$

where $w_g$ is the output of the filter.


## Acknowledgment

This paper is based on a Ph.D. Thesis presented to the Department of Aeronautical Engineering, Technion – Israel Institute of Technology, Haifa, Israel, by A. J. Grunwald. The research was sponsored by the Department of Research and Development, Ministry of Defense, Israel.


## References


[1] Grunwald, A. J. and Merhav, S. J., "Vehicular Control by Visual Field Cues-Analytical Model and Experimental Validation," *IEEE Transactions on SMC*, Vol. 6, Dec. 1976.

[2] Grunwald, A. J. and Merhav, S. J., "A Study of Display Augmentation in Visually Controlled Vehicles," Technion, Aeronautical Engineering (TAE) Rept. No. 284, Haifa, Israel, May 1976.

[3] Naish, J. M., "Control Information in Visual Flight," *7th Annual Conference on Manual Control*, June 1971, p. 167.

[4] Naish, J. M., "Head-up Display for the Visual Approach," *8th Annual Conference on Manual Control*, May 1972, p. 159.

[5] Naish, J. M., "A Conformal Head-up Display for the Visual Approach," *9th Annual Conference on Manual Control*, May 1973, p. 133.

[6] Van Houtte, N.A.J., "A Perspective Glideslope Indicating System," *6th Annual Conference on Manual Control*, April 1970, p. 117.

[7] Palmer, E. and Wempe, T., "Pilot Performance with a Simulated Pictorial Landing Display Including Different Conditions of Resolution and Update Rate," *6th Annual Conference on Manual Control*, April 1970, p. 47.

[8] Palmer, E. and Wempe, T., "Pilot Performance with a Simulated ILS-Independent Pictorial Display," *7th Annual Conference on Manual Control*, June 1971, p. 139.

[9] Howard, J. C., "Display Requirements for the Final Approach and Landing Phase of an R.P.V. Mission," NASA TM X-62, 346, 1974.

[10] Howard, J. C., "The Influence of Loss of Visual Cues on Pilot Performance During the Final Approach and Landing Phase of a Remotely Piloted Vehicle Mission," *12th Annual Conference on Manual Control*, May 1976, p. 918.

[11] Weir, D. H. and McRuer, D. T., "A Theory for Driver Steering Control of Motor Vehicles," *Road User Characteristics*, Highway Research Record No. 247, 1968.

[12] Kleinman, D. L. and Baron, S., "Analytic Evaluation of Display Requirements for Approach to Landing," Bolt, Beranek, and Newman, Inc., Rept. No. 2075, March 1971.